The effects of charge transfers on the adsorption of CO on small Mo doped Pt clusters

Piero Ferrari,[a] Jan Vanbuel,[a] Nguyen Minh Tam,[b] Minh Tho Nguyen,[c] Sandy Gewinner,[d] Wieland Schöllkopf,[d] André Fielicke,[e] and Ewald Janssens*[a]

Abstract: The interaction of carbon monoxide with platinum alloy nanoparticles is an important problem in the context of fuel cell catalysis. In this work, molybdenum doped platinum clusters are studied in the gas phase, in order to obtain a better understanding of the fundamental nature of the Pt–CO interaction in the presence of a dopant atom. For this purpose, Pt_n^+ and $MoPt_{n-1}^+$ (n=3–7) clusters are studied by combined mass spectrometry and density functional theory calculations, making it possible to investigate the effects of Mo doping on the reactivity between platinum clusters and CO. In addition, infrared photodissociation spectroscopy is used to measure the stretching frequency of CO molecules adsorbed on Pt_n^+ and $MoPt_{n-1}^+$ (n=3-14), allowing an investigation of dopant induced charge redistributions within the clusters. These electronic charge transfers are correlated to the observed changes in reactivity.

Introduction

Platinum nanoparticles are widely used because of their high activity in a number of catalytic processes. For instance, in direct methanol (DMFC) and direct ethanol (DEFC) fuel cells, the alcohols are oxidized on a Pt catalyst, producing carbon dioxide, protons and electrons.[1,2] Fuel cells based on biofuels are a promising alternative for the combustion of fossil fuels as a source of energy, but the high reactivity of the platinum catalysts towards carbon monoxide is a major drawback. Carbon monoxide, which can be generated as reaction intermediate at the cell's anode, adsorbs on the surface of the Pt nanoparticles thereby reducing the number of active sites and thus the fuel cell's performance.[3] The interaction of CO with Pt has been studied intensively in the past decades, both experimentally and theoretically.[4-6] Diverse models have been suggested to describe the atop bonding mechanism between CO and Pt. Of the most used are the Blyholder model,[7] its more quantitative refinement the π-σ model,[8] and the d-band center model.[9,10] In the Blyholder model bonding is attributed to electron transfer from the occupied 5σ molecular orbital (MO) of CO to the empty Pt d-states and back-donation of electrons from occupied Pt d-states to the CO 2π* MO, which is unoccupied in the free CO molecule. The hybridized level between the empty Pt d-states and the 2π* MO of CO is antibonding in C–O, but bonding in Pt–C.[11]

Despite the extensive efforts of previous research, it remains challenging to experimentally probe the influence of the charge at the reactive site and of binding site coordination on the CO adsorption energy. This is a direct consequence of the difficulty to measure and control parameters such as the reactive site's charge state and coordination number.

Small clusters in the gas phase have proven to be ideal model systems to investigate fundamental aspects of complex reactions.[12-15] The good control over the cluster size, composition and charge state allows to distinguish the effects of these parameters on the studied reactions. Moreover, the high-vacuum conditions of a gas-phase experiment eliminate the contaminating agents that could affect the reaction mechanism. For small sized clusters, ranging from two to a few tens of atoms, direct comparison between experiment and quantum-chemical calculations is possible.[16,17]

Gas-phase experiments on complexes of CO with transition metal clusters, including Pt clusters, elucidated a correlation between the partial charge at the binding site and the cluster–CO interaction strength.[18-21] Hereto, infrared (IR) action spectroscopy was used to measure the stretching frequencies of the adsorbed CO molecules (ν_{CO}) as a function of the kind of atoms in the cluster, its size, and charge state. ν_{CO} proved to be a sensitive parameter for the electronic charge distribution within the clusters. Within the conceptual framework of the Blyholder model, a larger electronic density at the binding site enhances the back-donation to the CO 2π* antibonding MO, thereby weakening the C–O bond and lowering ν_{CO}.

A significant amount of research in the field of gas-phase clusters has been devoted to the influence of doping on the properties of clusters such as their structures,[22,23] optical responses,[24,25] and reactivity.[26,27] All these studies have shown that a single dopant atom can strongly influence the clusters' properties. This research is relevant in the context of fuel cells catalysts, since it is well-known that upon alloying the CO tolerance of platinum based fuel cells can be improved considerably.[3] In a recent combined mass spectrometry and density functional theory (DFT) study, some of the current

[a] Piero Ferrari, Jan Vanbuel, Prof. Dr. Ewald Janssens,
Laboratory of Solid State Physics and Magnetism
KU Leuven
Celestijnenlaan 200D, 3001 Leuven (Belgium)
E-mail: ewald.janssens@kuleuven.be
[b] Dr. Nguyen Minh Tam,
Computational Chemistry Research Group and Faculty of Applied Sciences, Ton Duc Thang University
Ho Chi Minh City (Vietnam)
[c] Prof. Dr. Minh Tho Nguyen,
Department of Chemistry, KU Leuven
Celestijnenlaan 200F, 3001 Leuven (Belgium)
[d] Sandy Gewinner, Dr. Wieland Schöllkopf,
Fritz-Haber-Institut der Max-Planck-Gesellschaft
Faradayweg 4-6, 14195 Berlin (Germany)
[e] Dr. André Fielicke,
Institut für Optik und Atomare Physik
Technische Universität Berlin
Hardenbergstraße 36, 10623 Berlin (Germany)

Supporting information for this article is given via a link at the end of the document

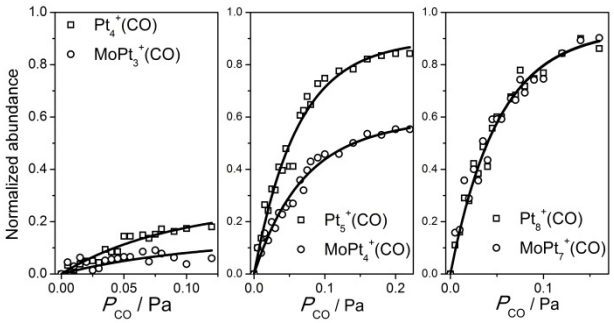

Figure 1. Three examples of normalized abundance as a function of the CO pressure in the reaction cell for Pt_n^+(CO) and $MoPt_{n-1}^+$(CO) (n = 4, 5 and 8). Fits of the experimental data using Eq. (3) are shown as continuous lines. The source temperature is kept at 130 K for these measurements.

authors studied the effect of doping on the reactivity of gas-phase Pt clusters (XPt_n^+; X = Mo, Nb, Sn, and Ag; 13 ≤ n ≤ 23) towards CO.[28] This work showed that a single dopant atom can reduce the interaction strength of Pt clusters with CO and that this effect depends on the type of dopant atom. More specifically, Mo and Nb doping reduced the CO adsorption energy, whereas only minor changes were induced by Ag and Sn doping.

In the current work we explore this intriguing behavior in more depth, focusing on correlated effects of Mo doping on electronic charge redistributions and the Pt clusters' reactivities towards CO. The reactions of Mo doped Pt_n^+ (3 ≤ n ≤ 14) clusters with CO are investigated in a low pressure collision cell by means of mass spectrometry and the CO stretching frequencies (ν_{CO}) of the cluster–CO complexes are measured using IR photodissociation spectroscopy. For interpretation of the experimental observations, DFT calculations are performed for Pt_n^+ and $MoPt_{n-1}^+$ (3 ≤ n ≤7).

Results and Discussion

Dissociation rates of cluster–CO complexes

Figure 1 illustrates the formation of metal cluster carbonyl complexes by interaction of the Pt clusters with CO in a low pressure collision cell. The pressure dependent formation of CO complexes by Pt_n^+ and $MoPt_{n-1}^+$ is shown for three sizes (n = 4,5 and 8). Kinetic data for other sizes are available as Supporting Information. The plotted quantity is the CO pressure (P_{CO}) dependent intensity of the cluster–CO signal in the mass spectra, normalized by the sum of the intensities of the bare cluster and its CO complex. A first observation is that for a given P_{CO}, the smallest clusters, Pt_4^+ and $MoPt_3^+$, form the least CO complexes. This behavior can easily be explained by the small heat capacity of those four-atom clusters. When a cluster–CO complex is formed, its heat of formation is redistributed over the vibrational degrees of freedom of the cluster. Small clusters, with few degrees of freedom, heat up more than larger clusters thereby reducing the lifetime of the cluster–CO complex as it is not stabilized by further collisions. Hence, these complexes have low intensities in the mass spectra.[28,29] Under the applied experimental conditions no CO complexes are observed for n ≤ 3. More interestingly, Figure 1 reveals a size dependent influence of the dopant atom on the CO-complex formation, which one can see by comparing pure and doped clusters with the same number of atoms. For n = 4 and 5, CO complex formation is reduced upon Mo doping, whereas no apparent change upon doping is seen for n = 8.

Quantitative information of the clusters' reactivity can be extracted from the kinetic data, by assuming the following reaction mechanism for cluster M:

$$\mathrm{M} + \mathrm{CO} \underset{k_f}{\overset{k_D}{\leftrightarrows}} \mathrm{M(CO)} \quad (1)$$

$$\mathrm{M(CO)} \xrightarrow{k_D} \mathrm{M} + \mathrm{CO} \quad (2)$$

where (1) and (2) represent the reactions in and after the collision cell, respectively.[26,29] k_f and k_D are the reaction rates for formation and dissociation of the CO complex, respectively. The coupled temperature dependent rate equations corresponding to (1) and (2) can be solved as a function of P_{CO}:

$$\frac{[\mathrm{M(CO)}]}{[\mathrm{M}]_0} = \frac{k_f P_{\mathrm{CO}}}{k_f P_{\mathrm{CO}} + k_D k_B T_{\mathrm{CO}}} e^{-k_D t_2} \left(1 - e^{-\left(k_f \frac{P_{\mathrm{CO}}}{k_B T_{\mathrm{CO}}} + k_D\right) t_1}\right) \quad (3)$$

where k_B is the Boltzmann constant, T_{CO} the temperature of the CO gas, and t_1 and t_2 the times the cluster spends inside the collision cell and between the cell and the entrance of the mass spectrometer, respectively. [M(CO)] / $[M]_0$ is the normalized abundance of the M(CO) complexes, relative to the initial amount of cluster M in the beam. A derivation of Eq. (3) can be found in the Supporting Information. Eq. (3) can be fit to the normalized abundances with k_D as sole fitting parameter if the forward reaction rate, k_f, is approximated by the hard-sphere collision rate.[29,30] These fits are presented in Figure 1 as solid lines. The satisfactory quality of the fits suggests that assuming k_f values from hard-sphere collision theory is a fairly good approximation. The extracted k_D values for cluster source temperatures of 130 K and 300 K are presented in Figure 2. Error bars on the k_D values include both fitting errors and model uncertainty on the k_f values (which were assumed to be hard-sphere collision rates) by assessing the change in k_D for a variation of the forward rates with 10%. Dissociation rates are higher at 300 K than at 130 K, which is expected since at a lower source temperature, the clusters are colder prior the interaction with CO and the dissociation rate after CO adsorption is lower. One can also note a general decrease in k_D for

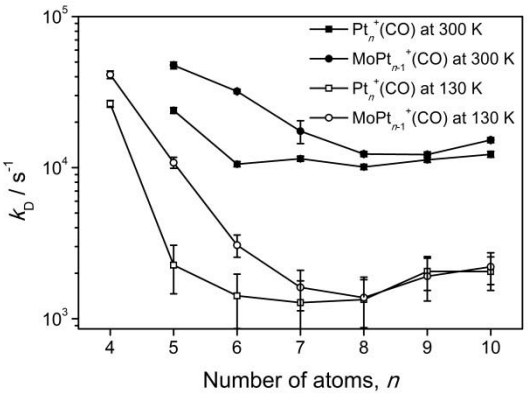

Figure 2. Dissociation rates k_D for the Pt_n^+(CO) and $MoPt_{n-1}^+$(CO) complexes (with n=4–10) at source temperatures of 130 K and 300 K.

increasing cluster size. This is due to the larger heat capacity of the larger clusters. Finally, and most importantly, upon Mo doping the dissociation rates for n = 4–7 increase (although at 130 K the k_D increase for n = 7 is not larger than the error bar). The enhancement is most pronounced for n = 5 and 6. For n = 8–10, k_D values do not change significantly upon doping under the applied experimental conditions. Assuming that changes in heat capacities are negligible upon doping (see Supporting Information for details), the observed increase in k_D induced by Mo can be attributed to a decrease in the CO binding energy, which will be discussed in more detail below.

Stretching frequencies of the adsorbed CO molecules

Complementary information about the effect of Mo doping on the interaction between Pt_n^+ clusters and CO is obtained by measurements of the internal stretching frequencies of adsorbed CO molecules, v_{CO}. Those are measured via photodissociation of the clusters–CO complexes following multiple photon absorption of infrared light from the free electron laser FHI FEL (see methods section). The photodissociation of Pt_n^+(CO) and $MoPt_{n-1}^+$(CO) (n = 3–6) complexes in the 2000–2150 cm^{-1} range is shown in Figure 3. The center of each observed band was determined by a Gaussian fit (solid lines in Figure 3) of the data.

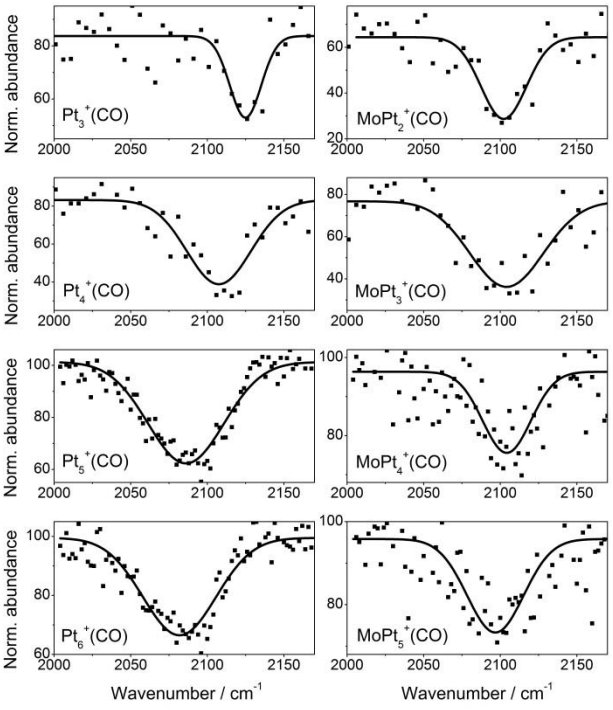

Figure 3. Photodissociation spectra of Pt_n^+(CO) and $MoPt_{n-1}^+$(CO) (n=3–6) in the 2000–2150 cm^{-1} range. Gaussian fits (solid lines) provide the center and the width of the bands corresponding to the CO stretching mode v_{CO}.

The results are summarized in Figure 4(a), showing v_{CO} up to n = 14. A zoom in the n = 3–7 size range is presented in Figure 4(b). For the pure Pt_n^+ clusters there is an overall decrease in v_{CO} with increasing cluster size. This behavior has been observed previously and is well understood in terms of the

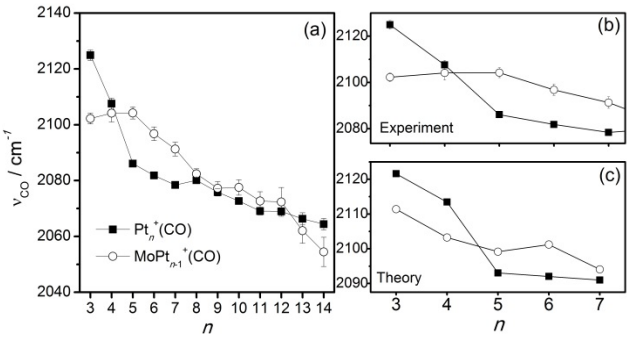

Figure 4. (a) Centre of the CO stretching bands for Pt_n^+(CO) (squares) and $MoPt_{n-1}^+$CO) (circles) (n=3–14) clusters. Error bars represent the uncertainty in the band center of the Gaussian fit. (b) Zoom of panel (a) in the N = 3-7 size region. (c) Center of the CO stretching mode on Pt_n^+ and $MoPt_{n-1}^+$ (n=3–7) clusters calculated by DFT.

electron density at the binding Pt site.[19] The overall positive charge of 1 e of the cationic cluster is distributed over a larger number of (surface) atoms for increasing cluster size, reducing the electron deficiency for each Pt atom. According to the Blyholder model, this produces a higher back-donation of electron density into the 2π* antibonding orbital of CO, reducing its vibrational frequency. For the doped $MoPt_{n-1}^+$(CO) clusters v_{CO} is found to be constant for the smaller clusters (n = 3-5) and to decrease for n > 5. Furthermore, the frequency shift observed for a given cluster size upon replacement of one Pt atom by a Mo atom is found to depend non-uniformly on the cluster size. One observes shifts to higher frequencies for n = 3,14, to lower frequencies for n = 5–7, or no apparent shifts (larger than the 1σ error) for n = 4,8-13. The size dependent shifts in frequency upon Mo doping can be traced back to the electron density at the Pt binding site, as will be described in the following sections.

Clusters' structures, CO adsorption energies and stretching frequencies

The most stable structures of the Pt_n^+(CO) and $MoPt_{n-1}^+$(CO) complexes with n = 3–7, as obtained by density functional theory (DFT) calculations, are presented in Figure 5. Minimum energy structures of the bare Pt_n^+ and $MoPt_{n-1}^+$ (n=3-7) clusters are provided as Supporting Information. For n = 3,5 and 7 the Mo only has minor effect on the geometry, while for n = 4 and 6 significant structural reorganization takes place, adopting slightly more planar structures upon doping. For all doped clusters, CO adsorbs atop at a Pt atom. Isomers with the CO molecule adsorbed on the Mo dopant were found to be at least 1 eV less stable than the structures of Figure 5. The calculated spin multiplicities and CO adsorption energies of the minimum energy configurations are detailed in Table 1.

Table 1. Spin multiplicities 2S+1, CO adsorption energies, CO stretching frequencies and Löwdin charges at the reactive Pt site of the Pt_n^+ and $MoPt_{n-1}^+$ clusters (n = 3-7)

Bare Cluster	2S+1 bare cluster	2S+1 CO complex	E_{ads} / eV	v_{CO} / cm^{-1}	Charge at Pt binding site
Pt_3^+	4	2	-2.42	2121	+0.32

$MoPt_2^+$	4	4	-2.45	2111	+0.22
Pt_4^+	4	4	-2.18	2113	+0.25
$MoPt_3^+$	4	4	-2.36	2103	+0.25
Pt_5^+	4	4	-2.49	2093	+0.20
$MoPt_4^+$	4	4	-2.09	2099	+0.26
Pt_6^+	6	6	-2.34	2092	+0.18
$MoPt_5^+$	4	4	-2.25	2101	+0.25
Pt_7^+	4	4	-2.74	2091	+0.17
$MoPt_6^+$	4	2	-2.36	2094	+0.21

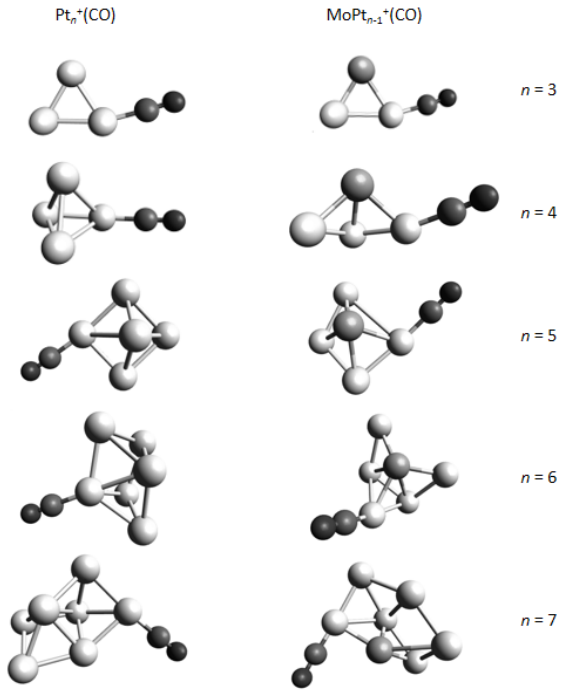

Figure 5. DFT calculated minimum-energy structures of Pt_n^+(CO) and $MoPt_{n-1}^+$(CO) with n=3–7. In increasing darkness, the drawn spheres present as Pt, Mo, C and O atoms.

Calculated CO stretching frequencies of Pt_n^+(CO) and $MoPt_{n-1}^+$(CO) are listed in Table 1 and compared in Figure 4(c). Consistent with the experiment, ν_{CO} of Pt_n^+(CO) is found to decrease with increasing cluster size and upon Mo doping ν_{CO} downshifts for n = 3 and 4 and upshifts for n = 5-7. Assuming that upon Mo doping the clusters' heat capacities are affected only slightly, the experimentally obtained CO dissociation rates k_D depend directly on E_{ads} ($E_{ads} = E_{clusters+CO} - E_{clusters} - E_{CO}$), i.e. larger k_D values correspond to complexes with weaker bound CO. A detailed description of the relation between k_D and E_{ads} is given in Ref. [28]. Based on the experimental results in Figure 2 one thus expects that Mo doping reduces the CO bonding for n = 5-7. Calculated results are in good agreement with those predictions: Mo doping reduces the CO adsorption energy from -2.49 to -2.09 eV for n = 5, from -2.34 to -2.25 eV for n = 6 and from -2.74 to -2.36 eV for n = 7. For the case of n = 4, however, for which experimental dissociation rates were measured and DFT calculations are available, it is not possible to infer a tendency in E_{ads} upon doping, due to the large uncertainty of the experiment.

The effect of electronic charge transfers

Considering the Blyholder model to describe the Pt–CO interaction, dopant induced electronic charge redistribution is expected to affect both the CO adsorption energy and the ν_{CO} stretching frequency. Therefore, atomic Löwdin charges were calculated for the clusters and their CO complexes. The local charges on the preferential CO adsorption site in the bare clusters are given in Table 1. For the monometallic Pt_n^+ clusters, the positive charge at the Pt binding site decreases monotonously with cluster size from +0.32 e for Pt_3^+ to +0.17 e for Pt_7^+. This decrease correlates with the redshift of ν_{CO} (Figure 4a) and confirms that the amount of back-donation, from the metal to CO, determines the redshift of ν_{CO}.

Mo doping has an effect on the Löwdin charges at the reactive Pt atom. A comparison of the charge distributions in Pt_3^+ and $MoPt_2^+$ shows that transfer of electron density from Mo to Pt reduces the positive charge at the Pt binding site of +0.32 e in Pt_3^+ to +0.22 e in $MoPt_2^+$. On the other hand, electron transfer from Pt to Mo is found for the larger cluster sizes (n = 5–7) in which the Pt atom binding to CO is more positively charged in $MoPt_{n-1}^+$ than in Pt_n^+. For n = 4 there is no apparent charge transfer.

The effect of Mo doping on the charge redistribution is visualized for n = 3 and n = 5 in Figure 6. In pure Pt clusters, the positive +1 e charge of the cationic cluster is almost equally distributed over the atoms, giving to each Pt a more positive charge in Pt_3^+ than in Pt_5^+. However, in $MoPt_2^+$, Mo donates electron density to Pt, ending up with a positive charge of +0.60 e, in opposition to $MoPt_5^+$, where transfer of electron density is seen from Pt to Mo, leaving Mo with the smaller charge of +0.12 e.

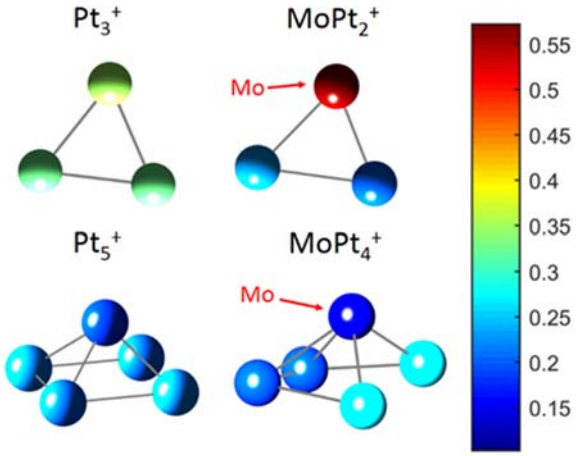

Figure 6. DFT calculated minimum-energy structures of Pt_n^+ and $MoPt_{n-1}^+$ (n = 3,5) clusters. The color code represents the atomic charge calculated using the Löwdin scheme.

These charge distributions are correlated with the observed shifts in ν_{CO} upon doping. If there is electron density transferred from Mo to Pt, a larger back-donation is accepted from Pt to the 2π* antibonding orbital of CO, decreasing the C–O bond strength and the CO stretching frequency. In contrast,

when electron density is transferred from Pt to Mo, less back-donation is possible and ν_{CO} increases. This close correlation between the atomic charge at the Pt binding site and ν_{CO} allows predictions about the charge transfers in the clusters to be made using the measured ν_{CO}. Such empirical models have been used before to understand trends on measured ν_{CO} values of CO adsorbed on different monometallic transition metal clusters in different charge states: $(Rh,Co,Ni)_n^{-/0/+}CO$,[18] $Co_n^+(H_2)_mCO$[21] and $(Ni,Pd,Pt)_n^{-/0/+}CO$.[19] The main assumption of the model is that ν_{CO} is mainly affected by the electron population at the 2π* antibonding orbital of CO, P(2π*). Since this antibonding orbital is populated by back-donation of electron charge from the reactive site to the CO molecule, P(2π*) is proportional to the excess charge at this site. One can propose a model that assumes a linear dependence between ν_{CO} and this excess charge. In an ideal metallic cluster the charge is equally distributed over the surface atoms and one gets:

$$\nu_{CO} = \nu_{CO}^{\infty} + \Delta\nu_{CO}^{ES} + \frac{dz}{n_s} \quad (4)$$

where ν_{CO}^{∞} represents the frequency in the limit of an infinite number of atoms on the cluster, $\Delta\nu_{CO}^{ES}$ the induced frequency shift due to the interaction of the dipole moment of CO with the electric field of the charged cluster (which shifts the charge distribution within the CO molecule), z the total charge of the cluster in e, d a proportionality constant, and n_s the number of surface atoms of the cluster (which for the small sizes studied here equals the number of atoms in the cluster, n). For $\Delta\nu_{CO}^{ES}$ the following expression is used:[18]

$$\Delta\nu_{CO}^{ES} = 1395\ cm^{-1}\left(z/r^2\right) \quad (5)$$

in which r is the distance from the center of the cluster to the center of the CO molecule. $r = r_{CL} + r_C + r_{CO}/2$ with r_{CL} the radius of the cluster, which is assumed spherical ($r_{CL} \approx r_M n^{1/3}$, with r_M the radius of the atom obtained from the bulk density), r_C the covalent radius of the carbon atom in a typical M–C bond (r_C = 0.52 Å) and r_{CO} the C–O distance (r_{CO} = 1.15 Å). The pre-factor 1395 cm^{-1} is obtained from DFT simulations.[18] A fit of Eq. (4) to the experimentally measured ν_{CO} values is shown in Figure 7(a) and yields ν_{CO}^{∞} = 2035 ± 1 cm^{-1} and d = 146 ± 7 cm^{-1}.

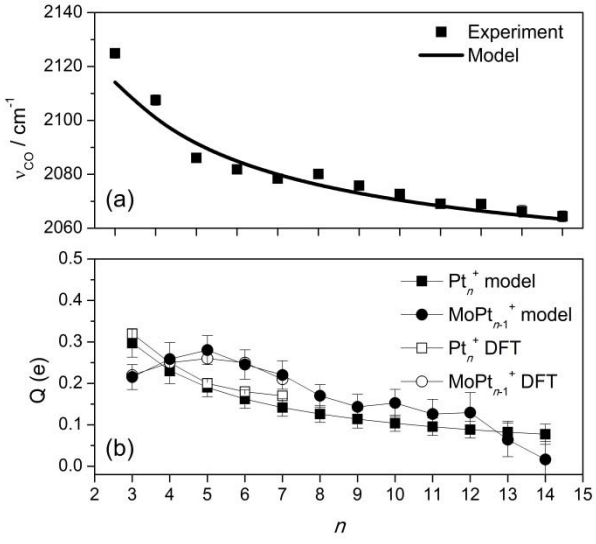

Figure 7. (a) Measured CO stretching frequencies, ν_{CO}, for pure $Pt_n^+(CO)$ (n=3-14) clusters (solid squares) and fit with Eq. (4) (solid line). (b) Charge at the CO binding site for Pt_n^+ and $MoPt_{n-1}^+$ clusters, obtained from the empirical model and from DFT calculations.

Since this fit predicts the smooth evolution of ν_{CO} with size, deviations between the fit and the measured values (Fig 7(a)) may be related to a non-uniform distribution of the charge. If this idea is correct Eq. (4) can again be used, but now to predict the local charges at the reactive Pt site. Therefore the term z/n_s in Eq. (4) is replaced by Q, the fractional charge at the reactive site and Q is calculated using the fitted ν_{CO}^{∞} and d values and the measured ν_{CO} for the pure Pt_n^+ and doped $MoPt_{n-1}^+$ clusters. The resulting Q values are shown in Figure 7(b) for n = 3–14 together with excess charges as obtained from DFT calculations for n = 3–7. Error bars on the modelled Q values are propagated from the uncertainties on fitted ν_{CO}^{∞} and d, and the measured v values using Eq. (4). For sizes for which DFT calculations are available, the fractional charges Q obtained by both methods agree well. Based on this good agreement for $n \leq 7$, the transfer of electron density can be estimated for the larger sizes using the measured ν_{CO}. In particular, for n = 14 ν_{CO} is redshifted upon Mo doping (see Figure 4-a). This suggests that the CO binding Pt site in $MoPt_{13}^+$ is less positively charged than that in Pt_{14}^+ and indicates an electron transfer from Mo to Pt. This was also seen in DFT calculations on the larger Pt_{19}^+CO and $MoPt_{18}^+CO$ clusters.[28] The empirical model yields local charges of +0.08 e and +0.02 e on the reactive sites in Pt_{14}^+CO and $MoPt_{13}^+CO$, respectively. Bader charge analysis, used in Ref. [28] for Pt_{19}^+CO and $MoPt_{18}^+CO$ gave local charges of +0.08 e and +0.01 e, respectively.

Finally, we discuss the correlation between transfer of electron density and CO binding energies. In the Blyholder interpretation bonding between CO and Pt is attributed to electron donation from the 5σ MO of CO to empty d-orbitals of Pt as well as the back-donation process. Thus, Mo dopant induced electron redistribution in the cluster may affect both interactions in opposite ways, requiring a detailed analysis of the electronic structure to make conclusions about the effect of doping. The top panel of Figure 8 presents the partial density of states (PDOS) of Pt_5^+CO and $MoPt_4^+$, projected on C, on O and on the Pt d-states. As a reference, the energies of the MOs of the free CO are indicated by vertical dashed lines. A first observation from the figure is the strong stabilization of the 4σ and 5σ MO's, which under the interaction with Pt are located at energies around -19 eV and -16.5 eV, respectively. The wave functions of these states are shown in the bottom panel of Figure 8. The stabilization is the strongest for the 5σ MO, which is ascribed to the electronic charge donation from CO to Pt. It is important to note that the 5σ stabilization is stronger in $MoPt_4^+$ than in Pt_5^+. This is a consequence of the electronic charge transfer from Pt to Mo in this cluster size, which leads to a larger density of unoccupied Pt d-states available to interact with CO. The enhanced 5σ stabilization seems to contradict the result that upon Mo doping the CO adsorption energy for this size is reduced. However, this effect gets over-compensated by the back-donation from occupied d-states of Pt to the antibonding 2π* MO of CO. Located between -14 eV and the Fermi level, E_F, several hybridized states of 2π* character are found in the PDOS spectra.[28] Since this MO is empty in the free CO, these hybridized states are ascribed as due to back-donation of

electron density from Pt to CO. Those hybridized states are antibonding for the C-O interaction, but bonding for the Pt-C bond.[8,11] An inspection of Figure 8 shows that the density of these states is larger in Pt_5^+ than in $MoPt_4^+$, especially near E_F due to the lower population of Pt d-states below the Fermi energy in the doped cluster, as a consequence of the Pt to Mo electron transfer. An integration of the density of states of C and O 1 eV below E_F gives around a 50% larger population in Pt_5^+ than in $MoPt_4^+$. So we can conclude that for Pt_5^+ the effect of charge redistribution upon Mo doping has a stronger influence on the back-donation than on the 5σ → *d* transfer, reducing the CO binding energy. A similar influence of Mo doping, i.e. a reduction of the CO adsorption energy, was observed previously for the Pt_{19}^+ cluster.[28] However, in that case, a transfer of electron density from Mo to Pt was observed and the 5σ

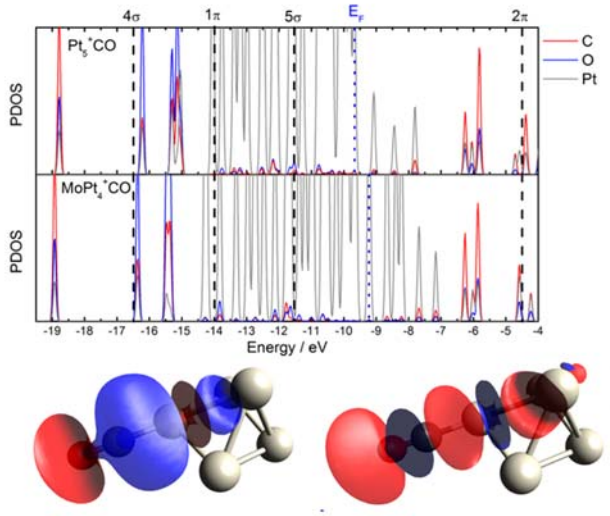

Figure 8. Top: partial density of states (PDOS) of Pt_5^+CO and $MoPt_4^+CO$. States projected onto C, O and Pt (d-states) are shown in red, blue and gray, respectively. In the figure, Fermi energies (E_F) are shown by a dotted line and the MOs of the free CO by dashed lines. Bottom: Wave functions of two selected MOs of Pt_5^+CO corresponding to the 4σ (right) and 5σ (left) MOs of free CO.

stabilization was more important than the 2π* hybridization.

Conclusions

In this work, the effect of a single Mo dopant atom on the bonding between CO and small gas-phase Pt_n^+ (*n*=3–14) clusters has been studied. Mass spectrometry was combined with density functional theory calculations in order to investigate the reactivity of the clusters. Theory and experiment are well in agreement, showing that, upon doping, CO binding energies were reduced, in particular for Pt_5^+, Pt_6^+ and Pt_7^+. In addition, electronic charge transfer induced by Mo doping was characterized by IR spectroscopic measurements of the CO stretching frequencies and charge population analysis calculations. Electron transfers were found to be size dependent. We found a correlation between the cluster-CO bond strength and the dopant induced electron transfer; for those sizes with a more positive charge at the Pt binding site, weaker CO binding energies were found. This demonstrates the importance of back-donation of electron density to the CO bonding mechanism. In the Blyholder model both the 5σ sigma donation and the 2π* back-donation are responsible for the Pt–CO bonding. However, these two mechanisms are affected oppositely by the charge at the atomic Pt binding site. This work has shown that in very small Mo doped Pt clusters the effect of reduced 2π* back-donation affects the CO binding more strongly than an enhanced 5σ sigma donation, resulting in an overall reduction of the CO binding energies. In previous studies performed on larger clusters a predominant 5σ sigma donation was found, in contrast to the cluster sizes studied here. This demonstrates the possibility to sensitively control donation and back-donation effects in the Pt-CO interaction by doping and cluster size.

CO reactivity measurements

The reactivity of the clusters towards CO was studied in a low-pressure collision cell,[29,30] installed in a molecular beam setup with a laser ablation cluster source and a time-of-flight mass spectrometer.[31] Rectangular Mo and Pt targets were ablated by two independent Nd:YAG lasers (532 nm, 10 Hz). Before ablation, He gas was introduced in the source by a pulsed valve (7 bar, 10 Hz) to trigger cluster formation. In this study the source was either maintained at room temperature or cooled down to 130 K by a continuous flow of liquid nitrogen. The cluster beam, composed of a mixture of pure Pt_n^+ and single doped $MoPt_n^+$ clusters (*n*=3-10), was exposed to CO gas in the collision cell. The pressure of CO (P_{CO}) was varied in the range between 0 and 0.2 Pa. The intensities of the clusters and their CO complexes are analyzed by time-of-flight mass spectrometry. Under the current conditions only cluster–CO complexes with maximally one CO molecule survive on the timescale of the experiment. Representative mass spectra are available as Supporting Information.

IR spectroscopy measurements

IR spectroscopy experiments were carried out in a dual-target dual-laser cluster setup connected to a beamline of the Infrared Free Electron Laser at the Fritz Haber Institute of the Max Planck Society in Berlin (FHI FEL).[32,33] A detailed description of the cluster source is available in Ref. [34] and its operation principle is similar to the source used for the CO reactivity measurements. The main difference is that for the IR spectroscopy experiments the CO gas is inserted via a pulsed valve into a reaction channel that is directly connected to the cluster source. The cluster source was kept at room temperature. Pure Pt_n^+ and single doped $MoPt_{n-1}^+$ clusters and their CO complexes were formed with a size distribution ranging from *n*=1 to *n*=14. After production, the cluster beam was collimated by a 2 mm diameter skimmer followed by a 1 mm diameter aperture where clusters interacted with the counter-propagating IR laser beam delivered by the FHI FEL with a repetition rate of 5 Hz. Finally, the cluster size distributions, with and without IR laser excitation, were analyzed by reflectron time-of-flight mass spectrometry. The wavelength of the FHI FEL was tuned in the range of the CO stretching mode (2000–2200 cm^{-1}).[19] An average pulse energy of 25 mJ and a step size of 2 cm^{-1} were used for the spectroscopy. The bandwidth or the IR radiation was 10-15 cm^{-1} (full width at half maximum).

Density functional theory calculations

Density functional theory (DFT) calculations for bare clusters, Pt_n^+ and $MoPt_{n-1}^+$, and their corresponding CO complexes, $Pt_n^+(CO)$ and $MoPt_{n-1}^+(CO)$ (n=3-7), were carried out using the TPSS exchange-correlation functional as implemented in the ORCA 3.0.3 software package.[35] For Pt and Mo atoms, 18 and 14 electrons were included in the valence, respectively, while the other electrons are described by the Stuttgart-Dresden ECP(def2-TZVP) pseudopotentials.[36] All electrons of C and O atoms were treated explicitly with the aug-cc-pVDZ basis set.[37] The selection of this computational level was motivated by the results of Ref. [38], in which the structures of small cationic pure Pt_n^+ clusters (n=3-5) were successfully assigned by a combined IR spectroscopy and DFT study. First minimum-energy structures of the bare clusters, Pt_n^+ and $MoPt_{n-1}^+$ (n=3-7), were searched, followed by an independent search of the corresponding CO complexes. This search carried out using the hybrid B3PW91 functional,[39,40] in conjunction with the aug-cc-pVTZ (for C and O) and aug-cc-pVTZ-pp (for Pt and Mo, pp stands for a set of pseudopotential) basis sets as implemented in the GAUSSIAN 09 package.[41] For each structure several spin states were tried and harmonic IR spectra were calculated. The coordinates of the obtained minimum-energy structures are given as Supporting Information. Löwdin populations were calculated to study atomic electronic charge distributions of the bare clusters and their CO complexes.

Acknowledgements

This work is supported by the Research Foundation-Flanders (FWO), by the KU Leuven Research Council (GOA/14/007) and the Deutsche Forschungsgemeinschaft (FI 893/3). P.F. acknowledges CONICyT for Becas Chile scholarship and J.V. thanks the FWO for financial support.

Keywords: platinum clusters • Mo doping • carbon monoxide • IR spectroscopy • reactivity

[1] A. Mehmood, M. Scibioh, J. Prabhuram, M. An, H. Ha, *J. Power Sources* **2015**, *297*, 224–241.
[2] S. Badwal, S. Giddey, A. Kulkarni, J. Goel, S. Basu, *Appl. Energy* **2015**, *145*, 80–103.
[3] S. Ehteshamia, S. Chan, *Electrochim. Acta* **2013**, *93*, 334–345.
[4] P. Glatzel, J. Singh, K. Kvashnina, J. van Bokhoven, *J. Am. Chem. Soc.* **2010**, *132*, 2555–2557.
[5] B. Hammer, Y. Morikawa, J. K. Nørskov, *Phys. Rev. Lett.* **1996**, *76*, 2141.
[6] P. Feibelman, B. Hammer, J. K. Nørskov, F. Wagner, M. Scheffler, R. Stumpf, R. Watwe, J. Dumesic, *J. Phys. Chem. B* **2001**, *105*, 4018–4025.
[7] G. Blyholder, *J. Phys. Chem.* **1964**, *68*, 2772–2777.
[8] N. Dimakis, M. Cowan, G. Hanson. E. Smotkin, *J. Phys. Chem. C* **2009**, *113*, 18730–18739.
[9] J. K. Nørskov, T. Bligaard, J. Rossmeisl, C. H. Christensen, *Nat. Chem.* **2009**, *1*, 37-46.
[10] R. Hoffmann, *Rev. Mod. Phys.* **1988**, *60*, 601.
[11] N. Dimakis, N. Navarro, T. Mion, E. Smotkin, *J. Phys. Chem. C* **2014**, *118*, 11711–11722.
[12] S. M. Lang, A. Frank, I. Fleischer, T. M. Bernhardt, *Eur. Phys. J. D* **2013**, *67*, 1-7.
[13] S. Zhou, J. Li, M. Schlangen, H. Schwarz, *Angew. Chem.* **2016**, *128*, 11036 –11039; *Angew. Chem. Int. Ed.* **2016**, *55*, 10877 –10880.
[14] S. M. Lang, I. Fleischer, T. M. Bernhardt, R. Barnett, U. Landman, *J. Am. Chem. Soc.* **2012**, *134*, 20654–20659.
[15] D. Justes, R. Mitrić, N. Moore, V. Bonačić-Koutecký, A. Castleman Jr., *J. Am. Chem. Soc.* **2003**, *125*, 6289–6299.
[16] H. Schwarz, *Angew. Chem.* **2015**, *127*, 10228 –10239; *Angew. Chem. Int. Ed.* **2015**, *54*,10090 –10100.
[17] S. Zhou, J. Li, M. Schlangen, H. Schwarz, *Acc. Chem. Res.* **2016**, *49*, 494–502.
[18] A. Fielicke, G. von Helden, G. Meijer, D. B. Pedersen, B. Simard, D. M. Rayner, *J. Chem. Phys.* **2006**, *124*, 194305.
[19] P. Gruene, A. Fielicke, G. Meijera, D. M. Rayner, *Phys. Chem. Chem. Phys.* **2008**,*10*, 6144-6149.
[20] A. Fielicke, P. Gruene, G. Meijer, D. M. Rayner, *Surf. Sci.* **2009**, *603*, 1427–1433.
[21] I. Swart, A. Fielicke, D. M. Rayner, G. Meijer, B. M. Weckhuysen, F. M. de Groot, *Angew. Chem.* 2007, *119*, 5411 –5414; *Angew. Chem. Int. Ed.* 2007, *46*, 5317 –5320.
[22] P. Gruene, A. Fielicke, G. Meijer, E. Janssens, V. T. Ngan, M. T. Nguyen, P. Lievens, *ChemPhysChem* **2008**, *9*, 703 – 706.
[23] L.D. Lloyd, R.L Johnston, S. Salhi, N.T. Wilson, *J. Mat. Chem.* **2004**, 14, 1691-1704.
[24] V. Kaydashev, P. Ferrari, C. Heard, E. Janssens, R. L. Johnston, P. Lievens, *Part. Part. Syst. Charact.* **2016**, *33*, 364–372.
[25] A. Shayeghi, C. J. Heard, R. L. Johnston, R. Schäfer, *J. Chem. Phys.* **2014**, *140*, 054312.
[26] H. Le, S. M. Lang, J. De Haeck, P. Lievens, E. Janssens, *Phys. Chem. Chem. Phys.* **2012**,*14*, 9350-9358.
[27] S. M. Lang, A. Frank, T. M. Bernhardt, *Int. J. Mass Spectrom.* **2013**,*15*, 365-371.
[28] P. Ferrari, L. M. Molina, V. E. Kaydashev, J. Alonso, P. Lievens, E. Janssens, *Angew. Chem.* **2016**, *128*, 11225–11229; *Angew. Chem. Int. Ed.* **2016**, *55*, 11059–11063.
[29] E. Janssens, H. Le, P. Lievens, *Chem. Eur. J.* **2015**, *21*, 15256 –15262.
[30] V. Kaydashev, E. Janssens, P. Lievens, *Int. J. Mass Spectrom.* **2015**, *379*, 133–138.
[31] W. Bouwen, P. Thoen, F. Vanhoutte, S. Bouckaert, F. Despa, H. Weidele, R. E. Silverans, P. Lievens, *Rev. Sci. Instrum.* **2000**, *71*, 54-58.
[32] W. Schöllkopf, S. Gewinner, H. Junkes, A. Paarmann, G. von Helden, H. Bluem, A. M. M. Todd, SPIE Conference Advances in X-ray Free-Electron Lasers Instrumentation III, Proc. of SPIE 9512, **2015**, 95121L.
[33] W. Schöllkopf, S. Gewinner, W. Erlebach, H. Junkes, A. Liedke, G. Meijer, A. Paarmann, G. von Helden, H. Bluem, D. Dowell, R. Lange, J. Rathke, A. M. M. Todd, L. M. Young, U. Lehnert, P. Michel, W. Seidel, R. Wünsch, S.C. Gottschalk, in: Proc. of the 36th Free Electron Laser Conference, Basel, Switzerland, **2014**, 629–634.
[34] N. Truong, M. Haertelt, B. Jaeger, S. Gewinner, W. Schöllkopf, A. Fielicke, O. Dopfer, *Int. J. Mass Spectrom.* **2016**, *395*, 1-6.
[35] F. Neese, *WIREs Comput. Mol. Sci.* **2012**, *2*, 73–78.
[36] F. Weigend, R. Ahlrichs, *Phys. Chem. Chem. Phys.* **2005**, *7*, 3297-3305.
[37] J. T. Dunning, *J. Chem. Phys.* **1989**, *90*, 1007.
[38] D. J. Harding, C. Kerpal, D. M. Rayner, A. Fielicke, *J. Chem. Phys.* **2012**, *136*, 211103.
[39] A. D. Becke, *J. Chem. Phys.* **1993**, *98*, 5648.
[40] J. P. Perdew, *In Electronic Structure of Solids '91*, (eds.: P. Ziesche, H. Eschig), Akademie Verlag, *Berlin*, **1991**, *p.11*.
[41] M. J. Frisch, G. W. Trucks, H. B. Schlegel et al., *GAUSSIAN 09, Revision B.01,* Gaussian, Inc., *Wallingford*, **2009**.